Notice of Retraction

"Perspective and Prediction of the Rule of High Temperature Melting of SiO_2 via Visual Analysis,"
by Yinghao Zhu; Ping He; Xiaozhen Ma; Kai Zhang; Heng Li; Haoyang Mi; Xing-Zhong Xiong; Zuxin Li and Yangmin Li
in IEEE Access, vol. 8, 2020

IEEE hereby retracts the content of this paper. It was been brought to the attention of the Editors that following publication, the authors were unable to verify the data after repeated experiments.

Due to the concerns regarding the validity of the content of the work, reasonable effort should be made to remove all past references to this paper, and refrain from future references to this paper.

IEEE Access
Multidisciplinary | Rapid Review | Open Access Journal

Received August 6, 2020, accepted August 31, 2020, date of publication September 4, 2020, date of current version September 30, 2020.

Digital Object Identifier 10.1109/ACCESS.2020.3021709

Perspective and Prediction of the Rule of High Temperature Melting of SiO_2 via Visual Analysis

YINGHAO ZHU[1], PING HE[2], XIAOZHEN MA[3], KAI ZHANG[4], HENG LI[5], HAOYANG MI[6], XING-ZHONG XIONG[7], ZUXIN LI[8], AND YANGMIN LI[9], (Senior Member, IEEE)

[1]Yisheng College, North China University of Science and Technology, Tangshan 063210, China
[2]School of Intelligent Systems Science and Engineering (Institute of Physical Internet), Jinan University, Zhuhai 519070, China
[3]Bangor College, Central South University of Forestry and Technology, Changsha 410004, China
[4]Yinlong Energy Company, Ltd., Gree Electric Appliances, Inc. of Zhuhai, Guangdong 519041, China
[5]Department of Building and Real Estate, The Hong Kong Polytechnic University, Hong Kong
[6]National Engineering Research Center for Advanced Polymer Processing Technology, Zhengzhou University, Zhengzhou 450000, China
[7]Artificial Intelligence Key Laboratory of Sichuan Province, Sichuan University of Science and Engineering, Zigong 643000, China
[8]School of Engineering, Huzhou University, Huzhou 313000, China
[9]Department of Industrial and Systems Engineering, The Hong Kong Polytechnic University, Hong Kong

Corresponding authors: Ping He (pinghecn@qq.com) and Kai Zhang (892760333@qq.com)

This work was supported in part by the National Natural Science Foundation of China under Grant 11705122, Grant 61902268, and Grant 51575544, in part by the Sichuan Science and Technology Program under Grant 2020YFH0124, Grant 2020YJ0368, Grant 2019YFSY0045, Grant 2018GZDZX0046, and Grant 2018JY0197, in part by the Hong Kong Scholars Program under Grant XJ2020047, in part by the Natural Science Foundation of Jinan University under Grant 2019QNGG26, in part by the Hong Kong Research Grants Council under Grant BRE/PolyU 152047/19E, Grant BRE/PolyU15210720, Grant BRE/PolyU 152099/18E, and Grant PolyU 15204719/18E, in part by the Natural Science Foundation of The Hong Kong Polytechnic University under Grant G-YW3X, in part by the Special Foundation of High-tech Zone of Zigong city under Grant 2021, in part by the Open Foundation of Artificial Intelligence Key Laboratory of Sichuan Province under Grant 2018RZJ01, in part by the Nature Science Foundation of Sichuan University of Science and Engineering under Grant 2017RCL52, and in part by the Zigong Science and Technology Program of China under Grant 2019YYJC03 and Grant 2019YYJC15.

ABSTRACT This paper focuses on how to see through the melting behavior of solid iron tailings in molten blast furnace slag and take a new non-contact visual analytical method to predict its melting law. The optimized convolution neural network (CNN) is used to track the moving target in charge coupled device (CCD) camera system efficiently and accurately, and the melting behavior of SiO_2 is described by coordinate translation transformation theory. Hierarchical agglomerative clustering (HAC) and delaunay triangulation were used to extract the characteristic parameters of the melting process of SiO_2. The prediction model of the melting rate of SiO_2 at high temperature was established by least square fitting (LSF) and dimensional analysis, and compared with the actual melting rate of SiO_2 obtained by experiments. The results show that the melting characteristics of SiO_2 at high temperature are in accordance with certain function rule. The performance of optimized CNN in terms of processing time and the accuracy are significantly improved, and the fusion rate prediction model of SiO_2 is verified by 100% accuracy. It provides theoretical support and model basis for the improvement of slag cotton preparation technology.

INDEX TERMS Melting rate, target tracking, feature extraction, dimensional analysis, best match.

I. INTRODUCTION

Motivation: At present, there are many disadvantages in the process and utilization of blast furnace slag, such as low utilization rate, environmental pollution and so on [1]. With the rapid development of intelligent manufacturing 2025 [2] to industrial transformation, artificial intelligence appears frequently in the industrial field. Among those, the mathematical model constructed via algorithm provides the bridge between artificial intelligence and engineering practice. Chinese Premier Keqiang Li emphasized on strengthening the utilization of mineral resources in the first executive meeting of the State Council in 2018. The iron and steel industry ranks first in China's high energy consumption industry. The blast furnace ironmaking process is the source of the iron and steel production chain [3]. It accounts for 70% of the total energy consumption of iron and steel production, which is a disaster area of energy conservation and emission reduction [4]. There is a lack of research on the dissolution behavior of SiO_2 and other slag in China. SiO_2 is the main component of solid iron

The associate editor coordinating the review of this manuscript and approving it for publication was Eduardo Rosa-Molinar.

tailings in blast furnace slag [5]. It is important to study the melting law of SiO_2 at high temperature for promoting the development of iron and steel industry in China. The purpose of this paper is to explore a new non-contact method, so as to see through the melting behavior of iron tailings at high temperature. It provides technical support for the process of iron tailing from blast furnace slag. This is of great innovative significance to the national blast furnace smelting industry.

Brief summary of prior literature: Over the past decade, in order to improve the utilization rate of blast furnace slag treatment process, and solve the serious environmental pollution of the process. There are many processing methods have been proposed for studying blast furnace slag. The bottom filtration method (OCP) was mainly used in China [5]. The Imbafa method (INBA) was mostly used in European countries and the United States [6]. Both of which were wet process [7]. They have the disadvantages of large area and high system investment. Based on the characteristics of the treatment method, chemical composition and mineral composition of blast furnace slag, there are different ways of treatment [8]–[20]. Such as clsvof method based on k-wsst rayleigh flow model simulates the melting process of blast furnace slag at high temperature [8], metallurgical slag coal gasification system controls the slag outflow speed at the slag outlet to improve combustion efficiency [9], micro analysis and hot state experiment reduces the exhaust gas emission when the blast furnace slag melts [10]. Electric arc furnace melting and tempering method solves the way of sensible heat utilization of blast furnace slag and improves the high added value of blast furnace slag [11], blast furnace slag spray granulation method verified that the products of melting slag with high surface tension were mainly particles [12], X-ray diffraction analysis method under electronic scanning mirror eliminates the mineral structure effect of the sample and realizes the determination of SiO_2 content [13]. Among those, the optimized one is surface temperature and emissivity of flying blast furnace slag particles belong to transient measurement methods is better [14]–[16]. The biggest advantage for the above mentioned methods is continuous measurement and high accuracy [17], [18]. The results show that the surface emissivity of the slag particles is 0.89 when the surface temperature is 1402 °C. With the increasing awareness of energy conservation and emission reduction, many scholars gradually realize the broad prospect of blast furnace slag preparation of slag cotton [19], [20]. They explore the new technology of direct fibrosis of blast furnace slag preparation of slag cotton, and have made some achievements [21]–[29]. Basalt cotton was prepared by 60% blast furnace slag and 40% basalt, and its feasibility was verified [21]. The effect of compressive stress on the dielectric constant of feldspar is studied. The results show that the dielectric constant of feldspar at five high frequency points decreases obviously with the increase of compressive stress [22]. The blast furnace slag fiber was prepared by centrifugation, and the fiber products were finally prepared [23]. The results showed that carbon could promote the sodification of blast furnace slag containing titanium. When the rate of sodium reached 78%, it was stable [24]. The study on the synthesis of slow-release silicon potassium fertilizer with blast furnace slag as raw material [25], [26]. The experimental results showed that the synthesis conditions have no significant effect on the crystallinity of silicon potassium fertilizer [27]. A new nonlinear unmixing method (NBRU) was used to retrieve the best spatial distribution of seven minerals from hyperspectral data and evaluate the mineral abundance performance [28]. Through the influence of different mineral additives on the complex permittivity and electrical modulus of polyaniline, the experimental results show that low cost sodium metasilicate has a significant impact on the dielectric properties of polyaniline [29]. The methods of [8]–[13] described in this paper are all completed in the laboratory. They are difficult to simulate the actual industrial environment temperature and easy to produce false laws. No matter how the utilization method of blast furnace slag changes on the original basis. The melting behavior of perspective flux at high temperature is very important. It is the key technology of iron tailings tempering.

Recently, with the development of industry 4.0 and intelligent manufacturing, industrial transformation has been promoted rapidly. The solution of blast furnace slag smelting problem is more inclined to the innovative use of the model. Algorithm is the foundation of building mathematical model [30]. For energy conservation and pollution reduction, the solution of blast furnace slag smelting problem is more inclined to use the theoretical model to predict the melting behavior in the blast furnace slag. Convolutional neural network (CNN) [31]–[34], region convolutional neural network (R-CNN) [35]–[37], fast R-CNN and support vector machine (SVM) [38], [39] have become popular in the field of target tracking and positioning [40], [41]. CNN and other methods have been used to extract the depth features and adaptively fuse them [42]. Eventually achieve the tracking algorithm for small targets, but the accuracy needs to be improved. For the accurate acquisition of image target, the principle of visual invariant feature and visual content capture is applied to solve this problem. Optical non-destructive testing (NDT) has an important application to non directly observable targets, especially terahertz technology opens a new direction of internal NDT because of its excellent penetration capability to most of non-metallic materials [43]. In the thermal imaging and multispectral imaging technology, a new color invariant image representation based on the existing gray-scale image enhancement technology [44], [45]. It has new enlightenment on the color information of the high temperature research on the melting of iron tailings. However, there is still a lack of innovative algorithm for iron tailings problem. Its high temperature melting law needs to be studied. The algorithm is based on artificial intelligence and applied to industrial problems. This will promote the development of the industrial field.

Contribution of this paper: On the basis of the above discussions, a visual analytical model based on CCD is

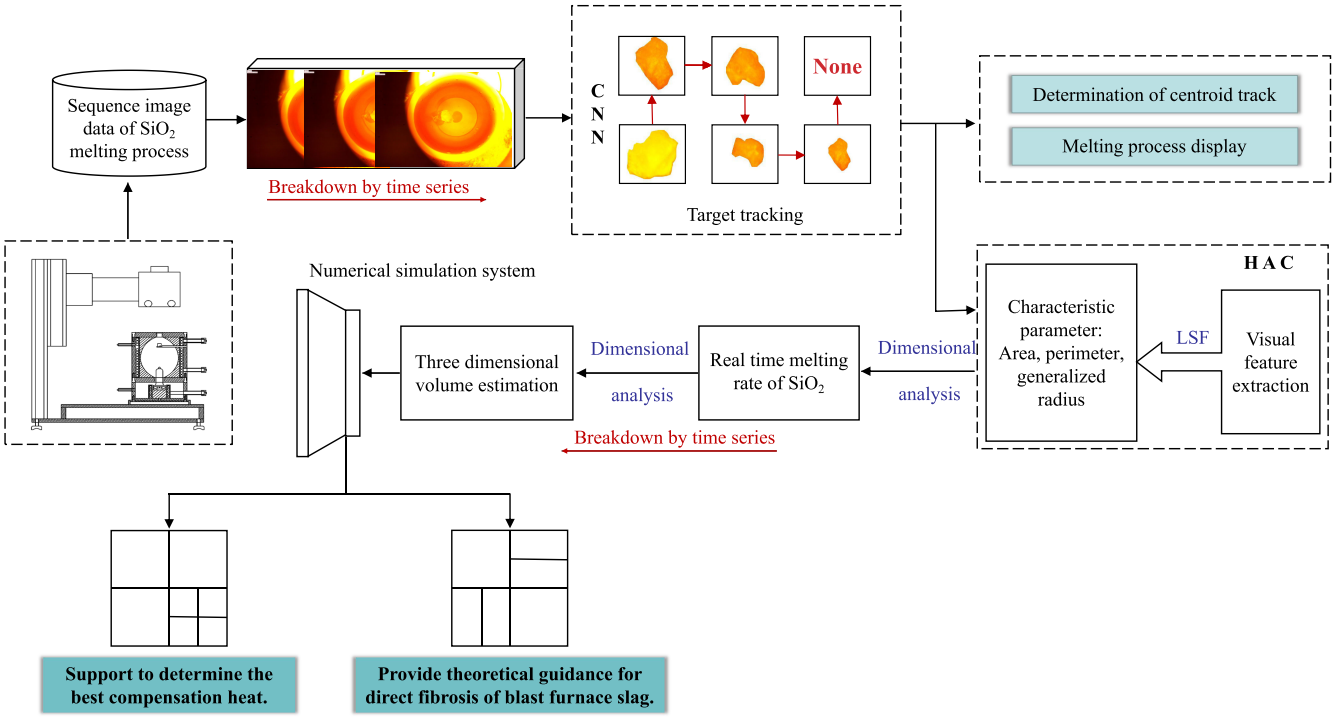

FIGURE 1. General technical process of perspective analysis.

proposed. It can realize the real-time image acquisition of iron tailings in high temperature environment. Less investment can complete the research of high temperature melting rule of ore. It also avoids the limitations of laboratory operation, and the original image sets are all in real industrial scene. The difficulty of this paper is to obtain and analysis the dynamic visual data characteristics of high temperature molten pool.

The main contributions of this paper focus on the following two aspects:

- A new perspective analysis method is used to realize the accurate tracking and feature extraction of dynamic target in high temperature furnace, the specific process is shown in Figure 1.
- The three-dimensiona (3D) volume estimation based on the two-dimensiona (2D) characteristic parameters of the target in time series images is realized, and the accurate prediction rate model of SiO_2 high-temperature melting is established.

Organization: The rest of this paper is organized as follows: In Section II, CNN accurately tracks the target, coordinates transformation transfers the center of mass coordinates to 2D plane, hierarchical agglomerative clustering (HAC) extracts the SiO_2 characteristic parameters, least square method and dimensional analysis establish the characteristic change equation, and finally get the prediction model of high-temperature melting of solid iron tailings. In Section III, CNN's software structure is optimized, and the change rule of characteristic parameters are analyzed. In Section IV, the final conclusions is obtained.

Notation: Q is the centroid position of the 2D image, q is the centroid position presented in the computer video, S is the area of the SiO_2 image, C is the perimeter of the SiO_2 image, R is the generalized circle radius of the SiO_2 image.

II. METHODOLOGY

This section explains the whole process of building visual analytical model. The centroid coordinates of the target are calculated by CNN target tracking and coordinate translation. HAC is taken to extract melting characteristic parameters of SiO_2. Finally, the least square method and dimensional analysis are taken to establish the melting rateprediction function of SiO_2.

A. TARGET IMAGE RECOGNITION

CNN [32] is the main representative of the deep learning theory. This algorithm is good at extracting the structural features of digital images. The images are used as the direct input, the depth feature of the image is recognized intelligently. It is a kind of algorithm that can realize the fast extraction and tracking of target features.

The molten SiO_2 particles will generate random walk in the crucible. CNN is used to intelligently identify and track the target in the sequence image, so as to achieve the accurate positioning of the target. It's necessary to consider both the target location and the dynamic migration of features with time series. In the melting process of SiO_2, the target area gradually decreases with time accumulation. The strategy of tracking the target is taken and the network is required

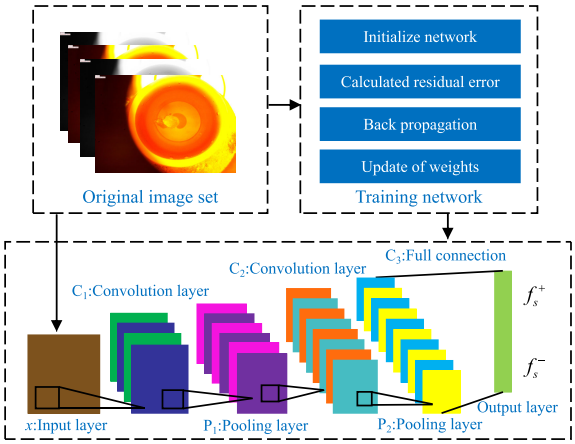

FIGURE 2. CNN structure for accurate tracking.

to have strong translation invariance. Based on the above analysis, according to the characteristics of SiO_2 image and target recognition, a CNN for SiO_2 target tracking is constructed. The input sample image gets the feature map in the convolution layer, then the pool layer is used for blur and generalization. Finally, the centroid position feature of the image is obtained. The network structure is shown in Figure 2.

In Figure 2, x is the image data input layer, C_1–C_3 is the convolution layer, P_1–P_2 is the pooling layer. In the input sample of network prediction, $f_x{}^+$ is the probability of target, $f_x{}^-$ is the probability of non target. In the training network, the image sample is convoluted with the filter. Then the output characteristics are obtained by the activation function. The output of neurons is shown as Equation (1).

$$x_j^l = f\left(\sum_{i\in M_j} x_j^{l-1}\cdot W_{ij}^l + b_j^l\right), \tag{1}$$

after the l-th convolution, the output of the j-th neuron is $x_j{}^l$; after the (l-1)-th convolution, the output of the i-th neuron is $x_j{}^{l-1}$; W_ij^l is the filter, $b_j{}^l$ is the bias function, M_j is the convolution layer of the current neuron, $f(\cdot)$ in Equation (1) is the nonlinear function which called sigmoid. Nonlinear factors are added to the activation function to preserve and map the features of the activated neurons to the next layer. There are significant differences between the target data set and the background data set, which can be regarded as a simple data set in classification. Therefore, the hidden layer of neural network is less needed in the target tracking method, the sigmod function doesn't appear gradient vanishing phenomenon, and its derivation is more simple and the operation is simplified.

After standardized sampling, this method can retain the invariant information to the greatest extent. In order to get high robustness and target recognition rate, the maximum sampling method is used to obtain the expression of sampling

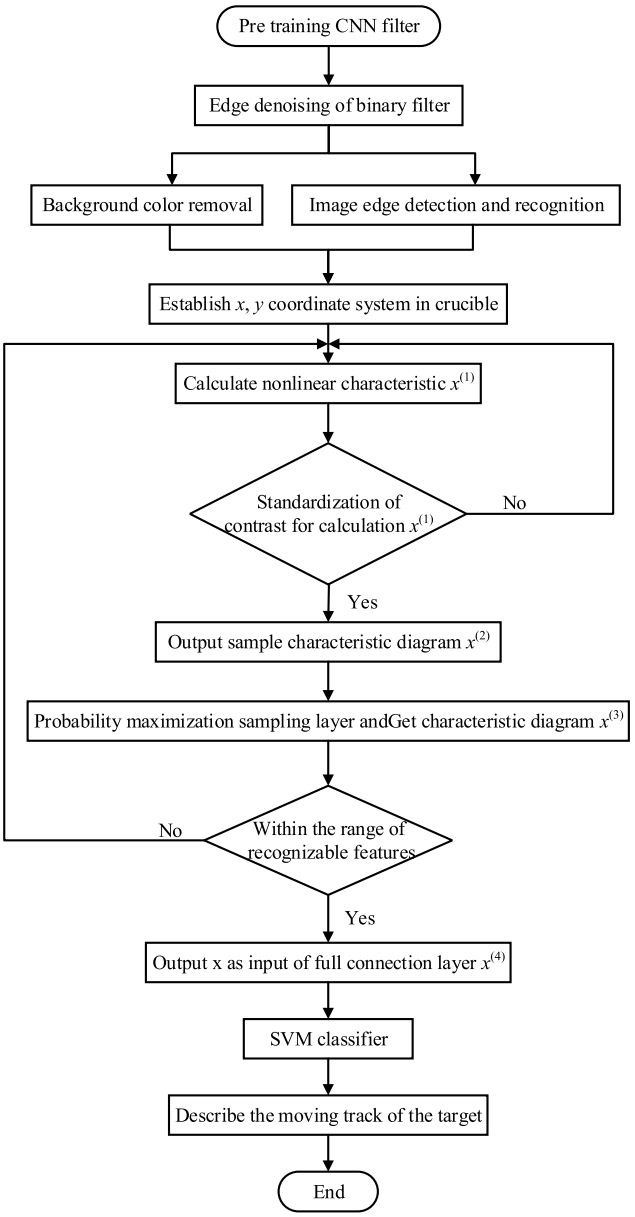

FIGURE 3. Flow chart of target tracking algorithm.

value P_α.

$$P(P_\alpha = 1|x) = \sum_{i,j\in B_\alpha} \exp\frac{\left[\left(W^k\cdot x\right)_{ij} + b_k\right]}{1 + \sum_{i,j\in B_\alpha}\left[\left(W^k\cdot x\right)_{ij} + b_k\right]}. \tag{2}$$

When any neuron B_α is turned on, the sample value P_α will react immediately; if any neuron B_α is not turned on, the sample value P_α will not respond. Based on the Equation (2), after the convolution neural network sampling, all the characteristic images are input into the full connection layer. After a hidden layer, the target features are obtained, and then the centroid position is obtained.

Three methods are used to recognize the target in the image. The final recognition results are shown in Table 1.

TABLE 1. Comparison results of algorithm accuracy.

Target recognition method	Number of test	Recognition rate	Average recognition rate
CNN	1	90.33%	91.38%
	2	95.00%	
	3	93.00%	
	4	87.00%	
	5	91.67%	
CNN+SVM	1	93.67%	94.24%
	2	97.00%	
	3	96.00%	
	4	91.00%	
	5	93.67%	
CNN+Random Forest	1	92.78%	93.83%
	2	95.80%	
	3	92.67%	
	4	94.56%	
	5	93.32%	

TABLE 2. Transformation of SiO_2 centroid coordinate system.

Times(s)	$x_i(mm)$	$y_i(mm)$	$x_i^{'}(mm)$	$y_i^{'}(mm)$
1	885	583	-185	3
2	911	589	-159	9
3	897	609	-173	29
4	903	617	-167	37
5	889	623	-181	43
6	893	620	-177	40
7	896	625	-174	45
8	895	619	-175	39
9	887	626	-183	46
10	885	627	-185	47
11	887	622	-183	42

The recognition accuracy of the combination of CNN and support vector machine (SVM) is obviously better than the other two methods, so the former is selected to track the iron tailings in the image.

Based on the CNN model, combined with the SVM classifier target tracking algorithm [46]. The implementation steps are shown in Figure 3. $x^{(l)}$ in Figure 3 is the eigenvalue of l-th convolution. It's calculated by Equation (1).

B. COORDINATE TRANSLATION TRANSFORMATION

In this experiment, the central position of the crucible is taken as the coordinate origin $(x_0, y_0) = (0, 0)$. The position of the center of mass is (x_1, y_1). The SiO_2 centroid coordinates obtained by CNN are translated in Equation (3).

$$\begin{aligned}(x_0 - a, y_0 - b) &= (0, 0)\,,\\ (x_i - a, y_i - b) &= \left(x_i', y_i'\right),\end{aligned} \tag{3}$$

where (x_0, y_0) is the central position of the crucible, $\boldsymbol{a}$ is the translation unit of the horizontal axis, $\boldsymbol{b}$ is the translation unit of the vertical axis, (x_i, y_i) is the centroid coordinate, (x_i', y_i') is the center of mass coordinate after translation transformation. Table 2 shows the partial centroids (pixel width of x, pixel width of y) and the transformed coordinates.

Based on the position of the object's center of mass, the track of tracking is visualized. Single mapping matrix is used to map target position in time series, SiO_2 trajectory can be observed clearly in CCD. In computer vision, the projection of 2D plane image is transformed to another plane by the homography matrix. The classical mapping is from 2D plane to camera video, which is defined as Equation (4). x, y and z represent three dimensions of 3D coordinates: abscissa, ordinate and vertical coordinate.

$$\widetilde{Q} = \begin{bmatrix} x \\ y \\ z \\ 1 \end{bmatrix}, \quad \widetilde{q} = \begin{bmatrix} x \\ y \\ 1 \end{bmatrix}. \tag{4}$$

There is a simplified representation of homography expressed as $\widetilde{q} = sH\widetilde{Q}$, where s is any scale, H is the projection of parameter matrix and the physical transformation of object plane in CCD. The physical transformation is expressed as the total influence of the correlation transformation part in the image.

$$W = [Z\ t]\,. \tag{5}$$

In Equation (5), Z represents the matrix size, t represents the column vector, and W is the physical transformation of the object. If the parameter transformation in CCD camera is defined as G, then the homography matrix is expressed as Equation (6). Where f_x, f_y, c_x and c_y are four camera internal parameters.

$$\widetilde{q} = sGW\widetilde{Q}, \quad G = \begin{bmatrix} f_x & 0 & c_x \\ 0 & f_y & c_y \\ 0 & 0 & 1 \end{bmatrix}. \tag{6}$$

Homography studies the projection from one plane to another, so after removing the z coordinate, it can be expressed as Equation (7), where r_1, r_2 and r_3 are three camera external parameters. X,Y and Z represent three dimensions of 3D coordinates of mapping surface: abscissa, ordinate and vertical coordinate.

$$\begin{bmatrix} x \\ y \\ 1 \end{bmatrix} = sG\,[r_1\ r_2\ r_3\ t] \begin{bmatrix} X \\ Y \\ 0 \\ 1 \end{bmatrix} = sG\,[r_1\ r_2\ t] \begin{bmatrix} X \\ Y \\ 1 \end{bmatrix}. \tag{7}$$

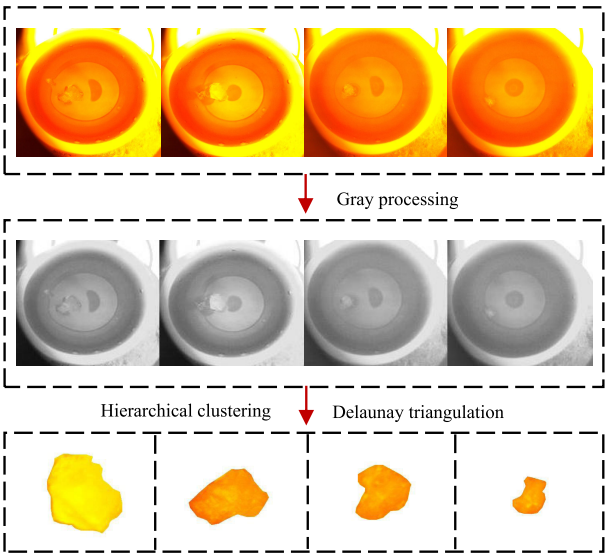

FIGURE 4. Image target extraction process.

Let $H = sG[r_1\ r_2\ t]$, then the homography matrix is expressed as $q = sHQ$.

C. IMAGE FEATURE EXTRACTION

With the help of high temperature furnace, it's easy to collect the melting image of SiO_2 at 1500 $^\circ C$. The acquisition interval is 1s. The image of dissolution process is opened by the drawing software, and the size of each image is 1792 × 1231. The PIL library in Python is used to intercept part of the image containing SiO_2 substance. Figure 4 shows the overall process of target extraction.

We extracte the target from the captured image, and transform into 2D array by RGB color histogram. HAC [47] firstly calculate the distance between the sample points, merge the closest points into the same class each time; then calculate the distance between classes and combine the closest classes into one category. Keep merging until synthesized a class. HAC is used to cluster images containing SiO_2 into 5 categories, and count the number of pixel values of each category. Figure 5 shows the statistical results of pixel values.

Delaunay triangulation is used to obtain the convex hull of the selected target point and the peripheral contour. As for triangulation: suppose E is a finite set of points in a 2D real field, edge e is a closed line segment composed of points in the point set as endpoints, and E is the set of e. So the triangulation of V_α, $T = (V_\alpha, E)$ is a plan G. This plan meets the following conditions:

- The edges in the floor plan don't contain any points in the point set except the endpoints.
- There are no intersecting edges.
- All faces in the plane plan are triangular, and the collection of all triangular faces is the convex hull of the scatter set V_α.

One edge e is assumed in E (with two endpoints α and β) satisfies the empty circle property, it can be called delaunay edge. If a triangulation T of point set V_α only

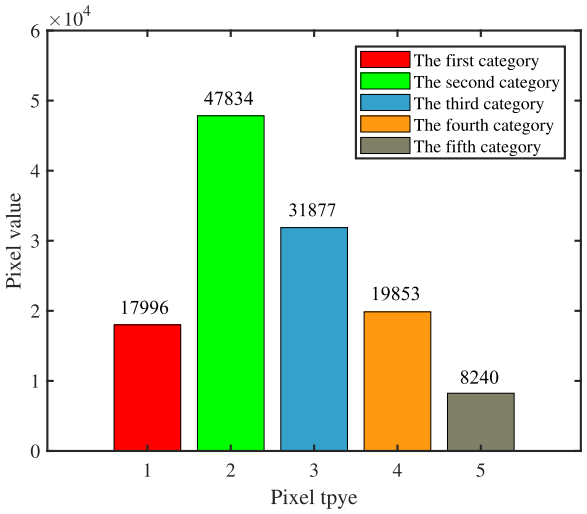

FIGURE 5. Results of HAC for target image pixels.

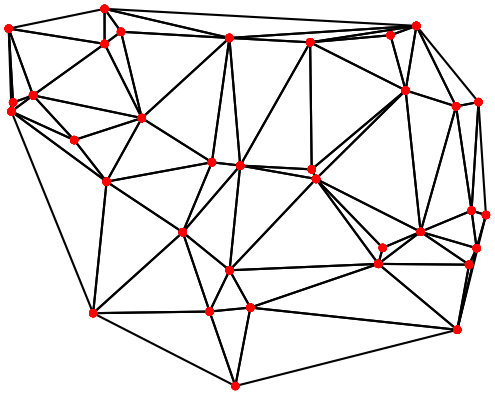

FIGURE 6. Join discrete points into a Delaunay triangle.

contains delaunay edges, the triangulation is called delaunay triangulation. If T is one triangulation of V_α, and the interior of the circumferential of each triangle in T doesn't contain any point in V_α, thus T is a delaunay triangulation of V_α. The delaunay triangular model formed by discrete points is as shown in Figure 6.

The steps of delaunay triangulation are as follows:

- Generate a large triangle containing all the points (whose fixed points are not in the set of points).
- Add a point P to the delaunay triangulated mesh, remove all the triangles that contain the point.
- Connect the P to all the visible points (no other edges will be intersected), and the resulting mesh will still satisfy the delaunay triangulation condition.
- Remove all edges associated with large triangles.

After edge feature extraction by HAC and delaunay triangulation, according to the outer diameter of the crucible is 8mm, we deduce the length of a single pixel value, then calculate the area of the captured image. The area of the intercepted image is calculated and multiplied the proportion of SiO_2 area in the captured image, and then the area of silica is gotten. Finally, the relationship between time and area is established. Partial data at 1500 $^\circ C$ is taken as an example to

calculate: the pixel value of the diameter is 1277, the length represented by each lattice is 0.006265.

The relations of area and perimeter in the characteristic parameters are expressed as: $S = \pi R^2$, $C = 2\pi R$. According to the relations of other characteristic parameters, R can be expressed as $R = 2S/C$.

During the melting process of SiO_2, the characteristic parameters will change with its melting. The real-time dynamic parameters of SiO_2 are defined as generalized radius R_n, perimeter C_n and area S_n. They represent the dynamic changes of S, C and R in time series, but the morphology of SiO_2 crystal is relatively stable when it melts, and its density basically remains unchanged, the characteristic parameters in each time state still conform to the law of $R = 2S/C$. Therefore, the generalized radius R_n in the time series can be solved by the Equation (8).

$$R_1 = \frac{2S_1}{C_1}, \quad R_2 = \frac{2S_2}{C_2}, \quad \ldots, \quad R_n = \frac{2S_n}{C_n}. \tag{8}$$

D. BEST MATCH FOR QUALITY CHANGE

The LSF finds the best function matching of data by minimizing the sum squares of errors [48]. In this paper, the least square algorithm is used to determine the change rule of SiO_2 particle area S, perimeter C and generalized radius R with time series. Data fitting is used to determine the mathematical expressions of functions $S(t)$, $C(t)$ and $R(t)$, so as to accurately describe the melting process of SiO_2.

The LSF can describe the function relationship between discrete points. The commonly used function models are exponential function $y = ae^{bx} + k$, logarithmic functio $y = bln + a$, power function $y = ax^b + k$, polynomial function $y = \sum a_i x^i$. In order to find the optimal mathematical expression, the goodness of fit is taken as the evaluation index. The optimal expression is the function with the largest fitting optimization. $S(t)$, $C(t)$ and $R(t)$ are the characteristics of melting change with time series. However, the direct parameter reflecting the melting process of SiO_2 is mass. For the analysis of pure SiO_2 particles, the volume is directly proportional to the mass. Length, area, volume and mass are all physical quantities under the unit system. Their transformation and estimation follow the general rule.

Dimensional analysis is a method to share the attributes of physical quantities and establish causality [49]. This study is taken as an example, the expressions of functions $S(t)$, $C(t)$ and $R(t)$ are known, the density of pure SiO_2 particles is ρ. According to dimensional analysis to determine the change rule $m(t)$ of SiO_2 particle mass.

Let $S(t)$, $C(t)$, $R(t)$, ρ and $m(t)$ be $f\ (S,\ C,\ R,\ \rho,\ M) = 0$. Their dimensional expressions are: $[S] = L^2$, $[C] = L$, $[R] = L$, $[\rho] = ML^{-3}$ and $[m] = M$, where L and M are basic dimensions, ρ is the density of SiO_2, m is the quality of SiO_2 and the dimensional matrix A is expressed as Equation (9),

$$A = \begin{bmatrix} 2 & 1 & 1 & -3 & 0 \\ 0 & 0 & 0 & 1 & 1 \\ S & C & R & \rho & m \end{bmatrix}. \tag{9}$$

The linear equations of Equation (9) are expressed as Equation (10).

$$\begin{cases} 2y_1 + y_2 + y_3 - 3y_4 = 0, \\ y_4 + y_5 = 0. \end{cases} \tag{10}$$

It can be seen in Equation (11).

$$\begin{aligned} m_1(t) &= k_1 \rho \pi R(t)^3, \\ m_2(t) &= k_2 \rho \pi \left(\frac{S(t)}{\pi}\right)^{\frac{3}{2}}, \\ m_3(t) &= k_3 \rho \pi \left(\frac{C(t)}{2\pi}\right). \end{aligned} \tag{11}$$

These are the three channels to obtain the mass change law of SiO_2 melting process. In order to reduce the error, the final estimated result is the average value of melting rate estimated by Equation (11).

III. RESULTS AND DISCUSSION

This section discusses the accuracy of CNN target tracking after optimization. The melting rules of the characteristic parameters of SiO_2 is summarized. The final prediction hit rate is 100%, which verify the validity of SiO_2 visual analytical model.

A. MOTION TRACK OF CENTER OF MASS

The advantages of CNN combined with the stability of SVM. The image features are extracted by using the trained convolution layer and pooling layer, and they are trained in SVM for classification operation. Its significance lies in using SVM to replace the full connection layer in convolution network. The experimental results show that the effect will be improved by 2%-3%, which is a considerable improvement and has a wide range of significance.

The specific reasons for using convolution as feature extraction and SVM as classifier are as follows:

- Due to the nature of convolution and pooling, the translation part of the image has no effect on the final feature vector. Therefore, the extracted features are more difficult to over fit. Moreover, because of the invariance of translation, it is meaningless to alter the translated characters, so it is unnecessary to modify the samples again.
- The feature extracted by CNN is more scientific than simple projection. It will not let feature extraction become the bottleneck of improving accuracy.
- Nonlinear mapping is the theoretical basis of SVM method. The inner product kernel function of SVM can replace the nonlinear mapping of high-dimensional space.
- Support vector is the training result of SVM, which plays a decisive role in SVM classification decision.
- The goal of SVM is to partition the feature space into the optimal hyperplane, and the idea of maximizing the classification margin is the core of SVM method.

CNN is a kind of special multilayer neural network. Its network structure has the characteristics of local connection

Algorithm 1 The Predicting Process of CNN

Initialize original image set as $\boldsymbol{X}$
Initialization noise threshold $\boldsymbol{h}$
Calculate a pixel point of image set
if a pixel value of an original image set exceeds threshold **then**
    remove the pixel value of an original image set
end if
Set edge detection operator as ***Sobel***;
Set the coordinate system of $\boldsymbol{x}, \boldsymbol{y}$;
Calculate Image centroid
while eighborhood volume integrations completed < Maximum value of convolutable neighborhood **do**
    for move convolution window **do**
        Update nonlinear features by Equation (1);
    end for
    Output nonlinear characteristics $\boldsymbol{x}^{(1)}$
    Calculate image local contrast
    if Contrast standardization complete **then**
        Output nonlinear characteristics $\boldsymbol{x}^{(2)}$
    end if
    Set pixel move position as $(\boldsymbol{a}, \boldsymbol{b})$;
    Set pixel current position as $(\boldsymbol{na}, \boldsymbol{nb})$;
    Set updated image set as $\boldsymbol{X}'$;
    if sqrt (na-a) + sqrt (nb-b) < sqrt (blur radius) **then**
        Output nonlinear characteristics $\boldsymbol{x}^{(3)}$
    end if
    Output nonlinear characteristics $\boldsymbol{x}^{(4)}$
end while
Calculate target trajectory
return $\boldsymbol{X}'$

and parameter sharing. Taking the network connection of LetNet-5 as an example, it has 7 layers (excluding the input layer). Each layer contains different training parameters. The convolution layer is a convolution kernel of 5×5. With a bias parameter, there are 26 training parameters. The subsampling layer is a 2×2 input domain, each subsampling node has only two training parameters. If the image of 32×32 pixels are input, the final convolution layer of LetNet-5 is C_3. The center of the receiving domain is connected with a 20×20 region of the input image center. In this way, although the training speed is accelerated, the image pixels collected by CCD are 1792×1231. Because of the characteristics of CNN computing, if the abovestructure is still used, the final data calculation will be huge. It's difficult to achieve the high efficiency of target tracking.

The following changes are made to the calculation unit of CNN image data. The configurable 2D convolution computing unit is used to realize the hardware acceleration requirement of the system. A 2D convolution computing unit is constructed with multi-level pipeline structure. The block kernel is recombined to realize convolution of any size. The central area of the image collected by CCD is cut to 256×256. The number of CNN input channels is set to 3, and the number of output channels is set to 96. The convolution kernel size F is 12×12, the step size S is 4, and the filling value P is 2. N is the output size of CNN, for the output size of the target image, the formula is N=(W-F+2P)/S+1=63. The number of neurons with the size of 96×63×63 after convolution is 381024.

The convolution kernel of 12×12 is beneficial to the feature extraction of target edge region, but its disadvantage is that the computational performance is reduced. If different convolution kernels are used for the feature maps of the same layer, the features of different scales can be obtained. If these features are combined, the features obtained will be better than the single convolution kernel. In order to avoid a large number of extra parameters, a 1×1 convolution kernel is introduced into the concept structure. The actual result is as follows:

The actual image is a 256 dimensional input, which directly passes through a 3×3×256 convolution layer to output a 256 dimensional feature map. Then the parameter quantity is 256×3×3×256 = 589824. If the input of 256 dimensions passes through a 1×1×64 convolution layer, then a 3×3×64 convolution layer, and finally a 1×1×256 convolution layer, the output 256 dimension is 256×1×1×64 + 64×3×3×64 + 64×1×1×256 = 69632. This method can reduce the parameters of the first operation to one ninth. CNN's prediction steps are shown in Algorithm 1.

Figure 7 is the mapping of image data to calculation unit. The large convolution window can be divided into

TABLE 3. Comparison results of data fitting methods.

Data fitting method	Performance index	Parameter 1	Parameter 2	Parameter 3
Least square fitting	SSE	1.4690	0.1408	0.0035
	RMSE	0.1373	0.0425	0.0067
	R^2	0.9289	0.9529	0.9536
	Adjusted R^2	0.9271	0.9533	0.9525
Rational approximation method	SSE	3.4650	0.3208	3.6450
	RMSE	0.2094	0.6373	0.0102
	R^2	0.8324	0.8928	0.8934
	Adjusted R^2	0.8302	0.8914	0.8921

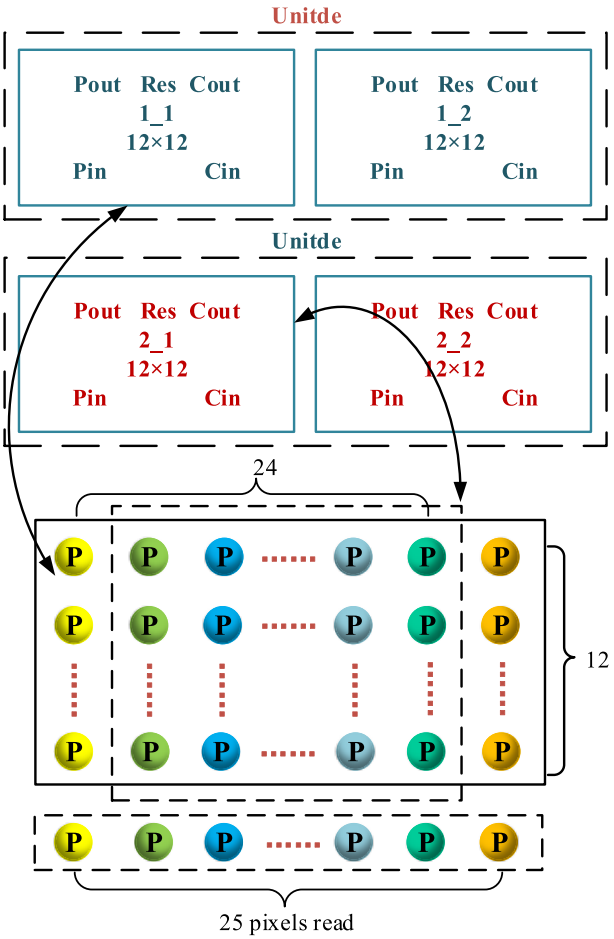

FIGURE 7. Optimization of CNN image to mapping unit.

several small convolution windows for many times calculation. This change greatly shortens the running time of the algorithm. After the comparison and analysis of the following algorithms (refer to Figure 8), it can be seen that the design also increases the accuracy of the calculation, and has a certain reference for other calculation intensive neighborhood processing algorithms.

CCD camera collects image data, then extracts edge features according to the image. Optimized CNN is used to locate and track the center of mass. The single strain transformation is used to obtain the coordinate transformation matrix. The corresponding matrix is able to convert the dynamic tracking of SiO_2. The optimized CNN is used to analyze the accuracy of target tracking. Refer to Figure 8 for target positioning accuracy comparison.

The results of CNN tracking accuracy of SiO_2 is compared in Figure 8, the unified conclusion can be obtained: the center of mass runs irregularly in the time sequence, but there is a phenomenon of sticking to the wall. SiO_2 particles will move gradually and irregularly towards the edge in the intial center. The final melting points are mostly in the sticking position, but the target prediction of the latter is more consistent. The actual data measured is combined with the experiment, the accuracy is higher. Through further analysis of the positioning results of the latter, the horizontal and vertical pixel value error is shown in Figure 9.

The coordinate error range in Figure 9 is within three pixel values, and the prediction accuracy is 95%. It is proved that the CNN has a high accuracy in predicting the path of particle. It can be used to acquire the real-time centroid position of sequence image accurately. It improves the operation speed of hierarchical clustering intelligent algorithm to extract target features.

B. MELTING LAW OF CHARACTERISTIC PARAMETERS

The characteristic parameter of SiO_2 particles in the extracted sequence image by HAC are shown in Table 4 and Table 5. The characteristic scatter points are analyzed and the appropriate function model should be determined. There are many ways to fit data. In this experiment, the scatter distribution of data is known. In order to compare the goodness of fit of the least square method, the rational number approximation method without destroying the data distribution law is selected. There are several performance indicators added, such as root square derror (RMSE) [50], sum of squares due to error (SSE), R^2 and Adjusted R^2 [51]. Figure 10, Figure 11 and Figure 12 are the renderings after the two methods are fitted. In the fitting of three characteristic parameters, the four performance indexes of the least square method are superior to the rational number approximation method all the time. Table 3 shows the comparison between the two fitting performance indexes.

The applicability of the two methods is studied by comparing several performance indexes. So Gaussian function is selected to fit scattered data by least square method. According to the characteristic parameters in Table 4 and Table 5, the fitting toolbox in MATLAB is selected for Gaussian function fitting to obtain the specific parameter values in the

TABLE 4. Extraction results of SiO_2 characteristic parameters.

Times(s)	Area(mm^2)	Perimeter(mm)	Generalized radius(mm)
0523	1.5187	0.703092853	0.111810274
0524	1.9037	0.770110266	0.124674416
0525	1.2620	0.636136522	0.100178057
0526	1.2727	0.631879405	0.101852147
0527	1.5187	0.702931944	0.111444236
0528	1.7647	0.748628346	0.120624986
0529	1.2193	0.622044131	0.098953444
0530	1.4332	0.668359291	0.107975833
0531	1.8396	0.758937708	0.121504848
0532	1.3476	0.659988952	0.103318427
0533	1.7433	0.746952839	0.117348949
0534	1.3904	0.657680284	0.106804646
0535	1.0053	0.559056618	0.091502393
0536	0.9947	0.565021002	0.090741246
0537	1.2620	0.636258303	0.101741042
0538	0.8984	0.537251114	0.085195288
0539	1.1016	0.596682993	0.093073691
0540	1.0160	0.560003762	0.090822165
0541	1.1658	0.603510127	0.096580288
0542	0.7914	0.501386051	0.080614221
0543	0.7273	0.479230511	0.076387858
0544	0.6096	0.443947852	0.070624281
0545	0.7487	0.485566980	0.078169721
0546	0.6203	0.451229092	0.070210966
0547	0.5668	0.434289579	0.069173050
0548	0.5882	0.426264101	0.068077115
0549	0.6631	0.458582571	0.072769192
0550	0.5882	0.432326135	0.069139729
0551	0.5455	0.409066738	0.065230291
0552	0.5882	0.440221082	0.068984121
0553	0.5348	0.404705453	0.064175499
0554	0.3743	0.346320766	0.055890079
0555	0.4492	0.386381144	0.061535217
0556	0.4385	0.368967215	0.058573803
0557	0.4706	0.391950978	0.060505504
0558	0.3529	0.344633627	0.054348790
0559	0.3743	0.343480204	0.056112292
0560	0.4599	0.384289474	0.059876623
0561	0.4278	0.376462543	0.058264536
0562	0.3636	0.339930399	0.054879356
0563	0.3102	0.307284837	0.049196617
0564	0.2674	0.287474588	0.045109750
0565	0.2888	0.294398824	0.047368580
0566	0.3529	0.344412701	0.054264945
0567	0.3529	0.329760817	0.052009501
0568	0.2781	0.300963948	0.048503199
0569	0.3529	0.339861303	0.052916360
0570	0.2888	0.309832717	0.047508593
0571	0.2674	0.293194842	0.046716678
0572	0.2032	0.259088004	0.038943406
0573	0.1925	0.257269729	0.039536328
0574	0.2460	0.273682159	0.045734167
0575	0.2995	0.317393182	0.048153188
0576	0.3422	0.335353920	0.052801763
0577	0.2460	0.278685120	0.044098394
0578	0.2246	0.270748076	0.042734840
0580	0.2032	0.254275948	0.041021709
0581	0.2674	0.256597011	0.047186361
0582	0.2353	0.280077110	0.044325110
0583	0.1604	0.233372785	0.037438147
0585	0.1711	0.226071082	0.037056802
0586	0.1070	0.187979328	0.030658641
0587	0.1070	0.176686467	0.028425363
0588	0.0856	0.157504454	0.025095361
0589	0.1176	0.187979328	0.031789307
0590	0.1711	0.233935055	0.037803469
0591	0.0535	0.138994050	0.019962820
0592	0.0963	0.184156823	0.028159911
0593	0.0749	0.155867221	0.024830529
0594	0.0535	0.127487805	0.021180745
0595	0.1070	0.183229362	0.029682752
0596	0.0428	0.112283753	0.018643435

TABLE 5. *(continued)* **Extraction results of SiO_2 characteristic parameters.**

Times(s)	Area(mm^2)	Perimeter(mm)	Generalized radius(mm)
0597	0.0428	0.124391066	0.017357255
0599	0.0428	0.124391066	0.018206073
0600	0.0749	0.158648928	0.024509394
0601	0.0428	0.123894800	0.017894617
0603	0.0321	0.095226481	0.016128383
0604	0.0107	0.058178750	0.009463020
0607	0.0107	0.059851193	0.009980013
0609	0.0107	0.051912504	0.009315639
0610	0.0107	0.063031045	0.010835020

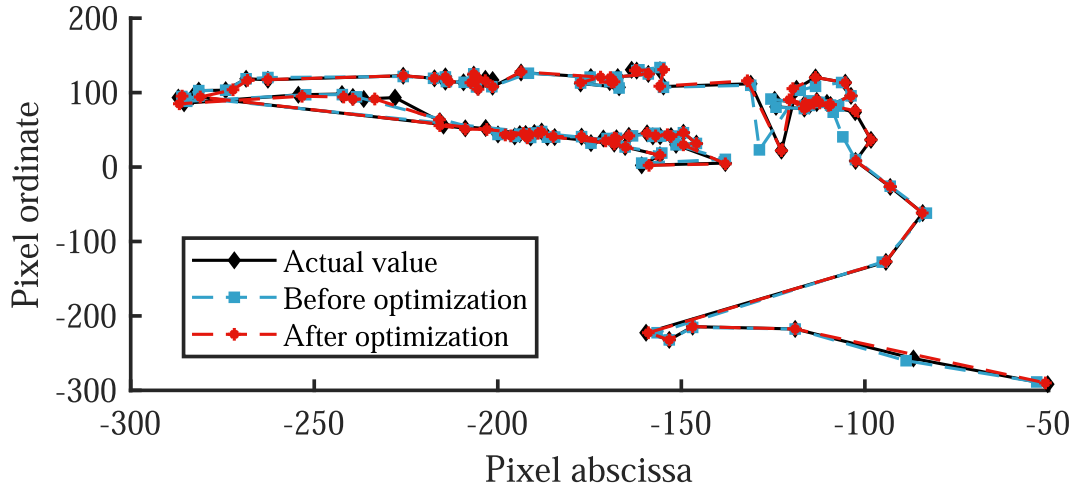

FIGURE 8. CNN target tracking trajectory.

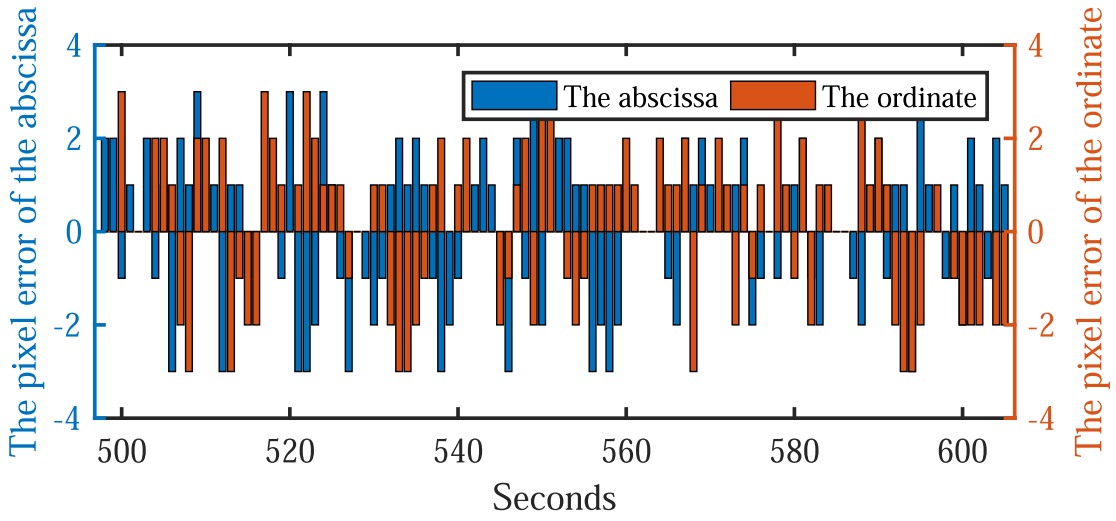

FIGURE 9. Coordinate pixel error.

Equation (11), (12) and (13). The functions for determining $S(t)$, $C(t)$ and $R(t)$ are as follows:

$$S(t) = 6.637 \exp\left[-\left(\frac{t-438.8}{72.78}\right)^2\right], \quad (12)$$

$$C(t) = 1.775 \exp\left[-\left(\frac{t-416.5}{114}\right)^2\right], \quad (13)$$

$$R(t) = 0.3127 \exp\left[-\left(\frac{t-408}{116.9}\right)^2\right]. \quad (14)$$

Among them, the goodness of fit of function $S(t)$ is 0.9289, the goodness of fit of function $C(t)$ is 0.9529, the goodness of fit of function $R(t)$ is 0.9536, and the effect is good. Figure 10, Figure 11 and Figure 12 are the fitting effect pictures.

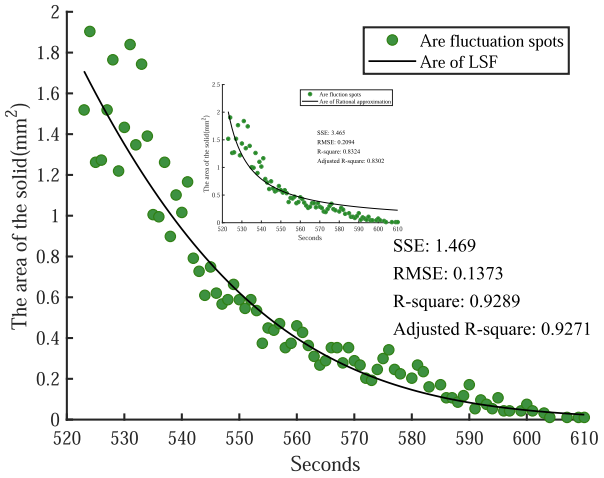

FIGURE 10. Variation of *S* with time.

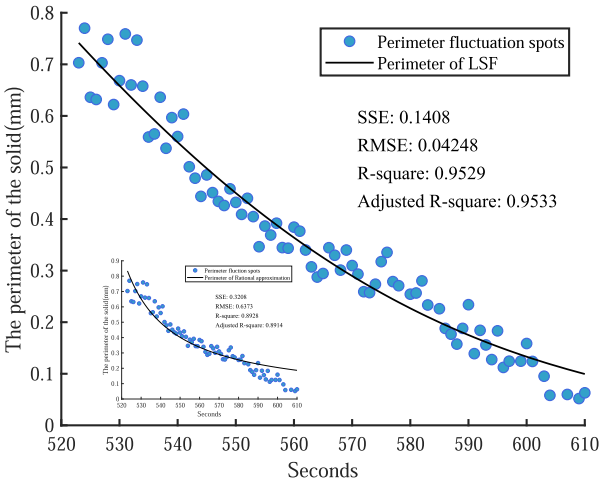

FIGURE 11. Variation of *C* with time.

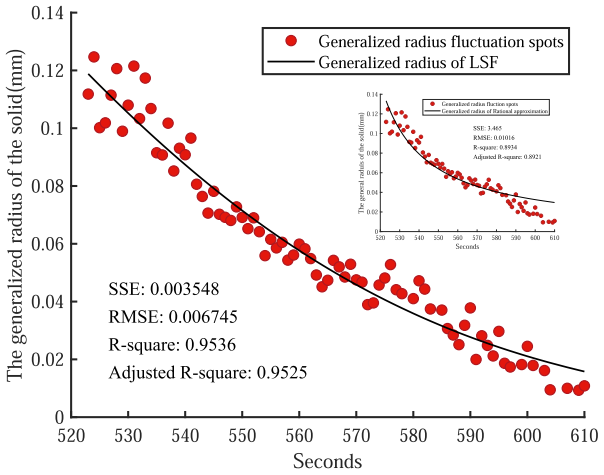

FIGURE 12. Variation of *R* with time.

C. ESTIMATION OF ACTUAL MELTING RATE

Mass is the physical quantity directly reflect the actual melting rate of SiO_2. The results of dimensional analysis are combined with characteristic parameter expressions, then

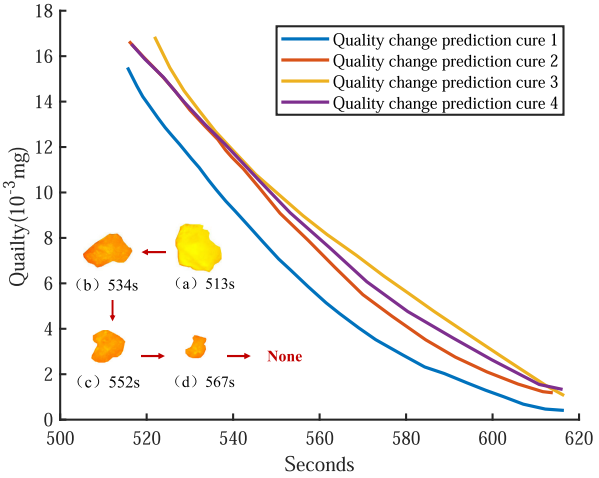

FIGURE 13. Quality change prediction curve.

the regular function of actual melting process is estimated. In order to eliminate the detection error, the mean value of the three estimated functions is taken as the SiO_2 quality prediction function.

According to Equation (11), (12), (13) and (14), only the solution coefficients k_1, k_2 and k_3 are needed in Equation (11). Based on the mass of SiO_2 before entering the crucible, the values of the three can be respectively calculated as: 6.637, 1.775 and 0.3127. In this process, select the quality prediction curve with SiO_2 density of 2.2 g/cm^3 [52].

The mass change prediction curve 1 in Figure 13 consists of curves 2, 3 and 4, which are expressed as Equation (15). By derivation of the above Equation (15), the actual melting rate function of silica is Equation (16).

$$m(t) = 0.01959 \exp\left[-\left(\frac{t-484.8}{76.21}\right)^2\right], \tag{15}$$

$$v(t) = -0.00542584\,(t-484.8) \exp\left[-\left(\frac{t-484.8}{72.21}\right)^2\right]. \tag{16}$$

The derivative of each point in the area change curve is calculated and the area change rate curve of SiO_2 is fitted. It can be seen from Figure 13 that the area of SiO_2 decreases gradually over time, but the rate of change slows down with the increase of time. Form the beginning to the end, it can be seen that the predicted curve 1 is closer to the actual situation. As there are two objectives for prediction of SiO_2 quality change, one is to obtain the melting rate in real time, the other is to determine when SiO_2 can completely melt. When the prediction function is determined, its melting rate can be obtained in real time. It's necessary to focus on whether the prediction function can accurately predict the end point, so as to ensure that less heat can be consumed under the premise of complete SiO_2 melting.

Based on the target of quality change prediction, the final prediction function is applied to predict the actual melting

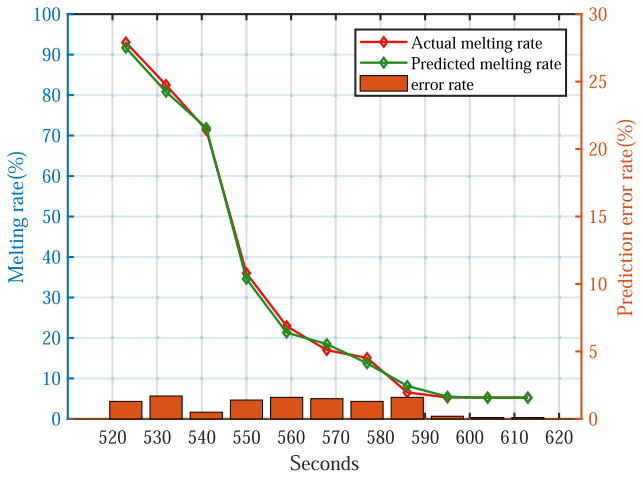

FIGURE 14. Prediction of melting process.

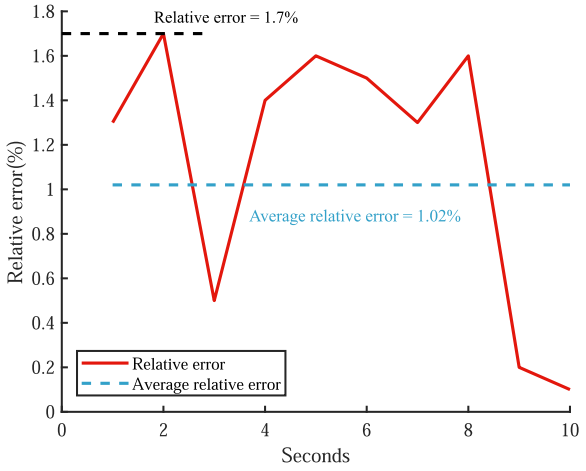

FIGURE 15. Relative error analysis.

end point. The actual melting rate of SiO_2 in Figure 14 is compared with the predicted melting rate, the results show that the trend of the two is almost the same. Through the relative error analysis, Figure 15 shows that the average relative error of SiO_2 predicted melting rate is 1.02%, the maximum relative error is less than 1.70%, and the accuracy is close to 100%, so that the validity of the visual analytical model can be verified.

IV. CONCLUSIONS

The purpose of this article is to investigate the melting behavior of solid iron tailings in high temperature molten pool. In this investigation, the prediction formula of SiO_2 actual melting rate was established by mathematical modeling method. The formula is expressed as: $v(t) = \delta(t - 484.8)\exp[-((t - 484.8)/72.21)^2]$, where δ is -0.00542584. Compared with the traditional research methods of iron tailings, this method can accurately predict the 3D melting law of iron tailings only according to the 2D parameter characteristics under the time series images. Compared with the real melting rate, the hit rate of the final SiO_2 melting rate prediction equation is 100%, which verifies the effectiveness of the visual analysis method. This article reveals the objective law of solvent dissolution in high temperature molten pool. The result solves the key problem of intelligent analysis of mathematical model, and provides a way to establish the matching function between iron tailings amount and compensation heat. In addition, the deep application of the achievements needs to be explored. The results can be connected with the metallurgical numerical simulation software, so as to realize the dynamic precision simulation of slag dissolution behavior. It offers theoretical support and technical support for the improvement of the preparation process of high added value slag cotton in the future.

ACKNOWLEDGMENT

The authors would like to thank Yinlong Energy Co., Ltd, Gree Electric Appliances, Inc. of Zhuhai, Guangdong, China for their valuable opinions and support. The relevant data was collected, processed, and completed in Yinlong Energy Co., Ltd. The relevant experiments of this manuscript have been greatly supported by Yinlong Energy Co., Ltd. Ms. K. Zhang coordinates all the work in an overall way. The authors would like to express their sincere appreciation to Prof. W. Wei, *Xi'an University of Technology*, for some valuable suggestions toward achieving the work of this paper.

REFERENCES

[1] I. H. Aziz, M. M. A. B. Abdullah, M. A. A. M. Salleh, E. A. Azimi, J. Chaiprapa, and A. V. Sandu, "Strength development of solely ground granulated blast furnace slag geopolymers," *Construct. Building Mater.*, vol. 250, Jul. 2020, Art. no. 118720.

[2] B. X. Sun, W. Pan, S. Yang, W. W. Deng, and S. J. Deng, "Research on the development strategy of Huai'an green intelligent manufacturing industry under the strategy of 'made in China 2025,'" *Sci. Technol. Innov.*, vol. 31, pp. 145–146, May 2019.

[3] K. C. Reddy, C. Gudur, and K. V. L. Subramaniam, "Study on the influences of silica and sodium in the alkali-activation of ground granulated blast furnace slag," *Construct. Building Mater.*, vol. 257, Oct. 2020, Art. no. 119514.

[4] Z. X. Zhang, "Energy consumption analysis of smelting reduction and blast furnace ironmaking," *Mod. Metall.*, vol. 47, no. 1, pp. 31–33, Feb. 2019.

[5] R. Arjmand, M. Massinaei, and A. Behnamfard, "Improving flocculation and dewatering performance of iron tailings thickeners," *J. Water Process Eng.*, vol. 31, Oct. 2019, Art. no. 100873.

[6] V. Yuthawong, I. Kasuga, F. Kurisu, and H. Furumai, "Molecular-level changes in dissolved organic matter compositions in lake inba water during $KMnO_4$ oxidation: Assessment by orbitrap mass spectrometry," *J. Water Environ. Technol.*, vol. 17, no. 1, pp. 27–39, Oct. 2019.

[7] J. Kwon, D. Lee, D. Yoo, S. Park, H. R. Cha, H. Kwon, J. Lee, and D. Lee, "Enhancement of magnetic properties of hot pressed/die-upset Dy-free Nd–Fe–B magnets with Cu/Nd coating by wet process," *Rare Met.*, vol. 39, no. 8, pp. 48–54, Feb. 2020.

[8] M. Z. Yu, H. Chang, A. J. Hu, X. J. Fan, B. Y. Xu, and J. G. Wang, "Study on the spray granulation method and simulation test of blast furnace slag," *J. Basic Sci. Eng.*, vol. 23, no. 4, pp. 836–841, Aug. 2015.

[9] A. G. Morozova, T. M. Lonzinger, V. A. Skotnikov, J. N. Sahu, G. G. Mikhailov, J. L. Schenk, A. Bhattacharyya, and Y. Kapelyushin, "Utilization of metallurgical slag with presence of novel CaO-MgO-SiO_2-Al_2O_3 as a composite sorbent for wastewater treatment contaminated by cerium," *J. Cleaner Prod.*, vol. 255, May 2020, Art. no. 120286.

[10] H. Abarghooei, H. Arabi, S. H. Seyedein, and B. Mirzakhani, "Modeling of steady state hot flow behavior of API-X70 microalloyed steel using genetic algorithm and design of experiments," *Appl. Soft Comput.*, vol. 52, pp. 471–477, Mar. 2017.

[11] T. Meier, V. Logar, T. Echterhof, I. Å. Krjanc, and H. Pfeifer, "Modelling and simulation of the melting process in electric arc furnaces—Influence of numerical solution methods," *Steel Res. Int.*, vol. 87, no. 5, pp. 581–588, May 2016.

[12] S. K. Tripathy, J. Dasu, Y. R. Murthy, G. Kapure, A. R. Pal, and L. O. Filippov, "Utilisation perspective on water quenched and air-cooled blast furnace slags," *J. Cleaner Prod.*, vol. 262, Jul. 2020, Art. no. 121354.

[13] Y. Long, P. P. Du, Z. H. Li, L. J. Zhang, and Y. Y. Zhang, "Preparation of slag cotton by direct fibrosis of blast furnace slag," *Sci. Technol. Eng.*, vol. 15, no. 35, pp. 87–91, Dec. 2015.

[14] A. C. de Oliveira Dieguez, S. L. N. Oliveira, G. S. Araújo, and A. G. de Sousa Galdino, "Comparison of kambara reactor slag with blast furnace slag for portland cement industry applications," *J. Mater. Res. Technol.*, vol. 8, no. 3, pp. 2786–2795, May 2019.

[15] H. L. Keizer and P. Kleinebudde, "Elastic recovery in roll compaction simulation," *Int. J. Pharmaceutics*, vol. 573, Jan. 2020, Art. no. 118810.

[16] J. Liu, Q. Qin, and Q. Yu, "The effect of size distribution of slag particles obtained in dry granulation on blast furnace slag cement strength," *Powder Technol.*, vol. 362, pp. 32–36, Feb. 2020.

[17] J. P. Reddy, R. Phanse, and V. Nesarikar, "Parameter estimation for roller compaction process using an instrumented vector TF mini roller compactor," *Pharmaceutical Develop. Technol.*, vol. 24, no. 10, pp. 1250–1257, Nov. 2019.

[18] T. J. Park, K. H. Ko, J. H. Lee, S. Gupta, V. Sahajwalla, and B. C. Kim, "Coke size degradation and its reactivity across the tuyere regions in a large-scale blast furnace of Hyundai steel," *Metall. Mater. Trans. B*, vol. 51, no. 3, pp. 1282–1288, Jun. 2020.

[19] Y. Feng, J. Gao, D. Feng, and X. Zhang, "Modeling of the molten blast furnace slag particle deposition on the wall including phase change and heat transfer," *Appl. Energy*, vol. 248, pp. 288–298, Aug. 2019.

[20] G. M. Kim, H. R. Khalid, H. J. Kim, and H. K. Lee, "Alkali activated slag pastes with surface-modified blast furnace slag," *Cement Concrete Composites*, vol. 76, pp. 39–47, Feb. 2017.

[21] S. Süsler, H. Kurtaran, H. S. Türkmen, Z. Kazancı, and V. Lopresto, "An experimentally validated numerical method for investigating the air blast response of basalt composite plates," *Mech. Adv. Mater. Struct.*, vol. 27, no. 6, pp. 441–454, Mar. 2020.

[22] W. Mao, L. Wu, and Y. Qi, "Impact of compressive stress on microwave dielectric properties of feldspar specimen," *IEEE Trans. Geosci. Remote Sens.*, vol. 58, no. 2, pp. 1398–1408, Feb. 2020.

[23] D. C. Ju, J. Y. Qiu, M. R. Xu, J. Zhang, H. F. Wang, and Y. H. Qi, "Effect of carbon on the thermodynamics and the rate of sodium reaction of titanium bearing blast furnace slag," *J. Iron Steel Res. Int.*, vol. 53, no. 1, pp. 88–93, Jan. 2018.

[24] D. Shishin, T. Hidayat, U. Sultana, M. Shevchenko, and E. Jak, "Experimental study and thermodynamic calculations of the distribution of Ag, Au, Bi, and Zn between Pb metal and Pb–Fe–O–Si slag," *J. Sustain. Metall.*, vol. 6, no. 1, pp. 68–77, Mar. 2020.

[25] O. Y. Bayraktar, "The possibility of fly ash and blast furnace slag disposal by using these environmental wastes as substitutes in portland cement," *Environ. Monitor. Assessment*, vol. 191, no. 9, pp. 1–12, Sep. 2019.

[26] J.-H. Ahn, H. Leeghim, and C.-Y. Lee, "Resistance characteristics and particle arrangement of smart paint for surface temperature sensor," *J. Nanosci. Nanotechnol.*, vol. 20, no. 7, pp. 4263–4266, Jul. 2020.

[27] J. Zhang, D. L. Yan, Y. Y. Qi, P. F. Shen, H. J. Xu, and J. J. Gao, "Analysis of difficulties in the treatment and utilization of iron and steel smelting slag," *Iron Steel*, vol. 55, no. 1, pp. 1–5, Jan. 2020.

[28] K. Siebels, K. Goïta, and M. Germain, "Estimation of mineral abundance from hyperspectral data using a new supervised neighbor-band ratio unmixing approach," *IEEE Trans. Geosci. Remote Sens.*, early access, Mar. 26, 2020, doi: 10.1109/TGRS.2020.2969577.

[29] M. Kiliç, Y. Karabul, Z. G. Özdemir, B. S. Misirlioğlu, and O. Içelli, "Improved dielectric and electrical properties of PANI achieved by using low cost mineral additive," *IEEE Trans. Dielectr. Electr. Insul.*, vol. 26, no. 1, pp. 300–307, Feb. 2019.

[30] Z. Tian, "Short-term wind speed prediction based on LMD and improved FA optimized combined kernel function LSSVM," *Eng. Appl. Artif. Intell.*, vol. 91, May 2020, Art. no. 103573.

[31] Z. Tian, G. Wang, Y. Ren, S. Li, and Y. Wang, "An adaptive online sequential extreme learning machine for short-term wind speed prediction based on improved artificial bee colony algorithm," *Neural Netw. World*, vol. 28, no. 3, pp. 191–212, 2018.

[32] D. Singhal, A. Gupta, A. Tripathi, and R. Kothari, "CNN-based multiple manipulation detector using frequency domain features of image residuals," *ACM Trans. Intell. Syst. Technol.*, vol. 11, no. 4, pp. 1–26, Jul. 2020.

[33] H. Jin, Y. Lian, and J. Hua, "Learning facial expressions with 3D mesh convolutional neural network," *ACM Trans. Intell. Syst. Technol.*, vol. 10, no. 1, pp. 1–22, Jan. 2019.

[34] Z. Tian, Y. Ren, and G. Wang, "Short-term wind speed prediction based on improved PSO algorithm optimized EM-ELM," *Energy Sources, A, Recovery, Utilization, Environ. Effects*, vol. 41, no. 1, pp. 26–46, Jan. 2019.

[35] G. L. Hung, M. S. B. Sahimi, H. Samma, T. A. Almohamad, and B. Lahasan, "Faster R-CNN deep learning model for pedestrian detection from drone images," *Social Netw. Comput. Sci.*, vol. 1, no. 2, pp. 17–23, Apr. 2020.

[36] F. Fang, L. Li, H. Zhu, and J.-H. Lim, "Combining faster R-CNN and model-driven clustering for elongated object detection," *IEEE Trans. Image Process.*, vol. 29, pp. 2052–2065, Jan. 2020.

[37] S.-S. Baek, J. Pyo, Y. Pachepsky, Y. Park, M. Ligaray, C.-Y. Ahn, Y.-H. Kim, J. A. Chun, and K. H. Cho, "Identification and enumeration of cyanobacteria species using a deep neural network," *Ecological Indicators*, vol. 115, Aug. 2020, Art. no. 106395.

[38] T. Zhongda, "Kernel principal component analysis-based least squares support vector machine optimized by improved grey wolf optimization algorithm and application in dynamic liquid level forecasting of beam pump," *Trans. Inst. Meas. Control*, vol. 42, no. 6, pp. 1135–1150, Apr. 2020.

[39] Z. Tian, S. Li, Y. Wang, and X. Wang, "Wind power prediction method based on hybrid kernel function support vector machine," *Wind Eng.*, vol. 42, no. 3, pp. 252–264, Jun. 2018.

[40] S. Bao, J. Meng, L. Sun, and Y. Liu, "Detection of ocean internal waves based on faster R-CNN in SAR images," *J. Oceanol. Limnol.*, vol. 38, no. 1, pp. 55–63, Jan. 2020.

[41] C. N. Meng and X. P. Zhao, "Webcam-based eye movement analysis using CNN," *IEEE Access*, vol. 5, pp. 19581–19587, Dec. 2017.

[42] J. P. Vasconez, J. Delpiano, S. Vougioukas, and F. A. Cheein, "Comparison of convolutional neural networks in fruit detection and counting: A comprehensive evaluation," *Comput. Electron. Agricult.*, vol. 173, Jun. 2020, Art. no. 105348.

[43] G. Finlayson, S. Hordley, G. Schaefer, and G. Yun Tian, "Illuminant and device invariant colour using histogram equalisation," *Pattern Recognit.*, vol. 38, no. 2, pp. 179–190, Feb. 2005.

[44] Z. W. Liu, B. Gao, and G. Y. Tian, "Natural crack diagnosis system based on novel L-shaped electromagnetic sensing thermography," *IEEE Trans. Ind. Electron.*, vol. 67, no. 11, pp. 9703–9714, Nov. 2020.

[45] Y.-K. Zhu, G.-Y. Tian, R.-S. Lu, and H. Zhang, "A review of optical NDT technologies," *Sensors*, vol. 11, no. 8, pp. 7773–7798, Aug. 2011.

[46] Z. D. Tian, Y. Ren, and G. Wang, "Short-term wind power prediction based on empirical mode decomposition and improved extreme learning machine," *J. Electr. Eng. Technol.*, vol. 13, no. 5, Sep. 2018, Art. no. 103573.

[47] S. Zafar, A. Bashir, and S. A. Chaudhry, "Mobility-aware hierarchical clustering in mobile wireless sensor networks," *IEEE Access*, vol. 7, pp. 20394–20403, Feb. 2019.

[48] M. S. Jia, J. M. Zhang, Y. X. Wu, and J. Wang, "Sound field reproduction via the alternating direction method of multipliers based lasso plus regularized least–square," *Int. J. Electr. Power Energy Syst.*, vol. 6, pp. 54550–54563, Sep. 2018.

[49] D. K. Dewi, Z. Abidin, B. Budiwantoro, and J. Malta, "Dimensional analysis of a rotor system through FRF using transfer function and finite element methods," *J. Mech. Sci. Technol.*, vol. 34, no. 5, pp. 1863–1870, May 2020.

[50] T. Zhongda, L. Shujiang, W. Yanhong, and S. Yi, "A prediction method based on wavelet transform and multiple models fusion for chaotic time series," *Chaos, Solitons Fractals*, vol. 98, pp. 158–172, May 2017.

[51] Z. D. Tian, S. J. Li, and Y. H. Wang, "A prediction approach using ensemble empirical mode decomposition-permutation entropy and regularized extreme learning machine for short-term wind speed," *Wind Energy*, vol. 23, no. 2, pp. 177–206, Feb. 2020.

[52] M. Hayashi, K. Suzuki, Y. Maeda, and T. Watanabe, "Effects of $2CaO{\cdot}SiO_2$ and $2CaO{\cdot}Al_2O_3{\cdot}SiO_2$ on primary slag melting of sinters in the cohesive zone of a blast furnace," *ISIJ Int.*, vol. 56, no. 2, pp. 220–225, Feb. 2016.

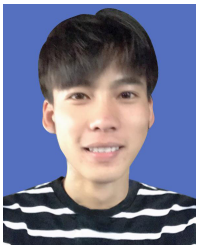

YINGHAO ZHU was born in Yantai, Shandong, China, in September 1998. He is currently pursuing the bachelor's degree with the North China University of Technology.

He founded Xinchuang Technology Ark studio, which has eight successful research and developing projects. Among them, the elderly care robot developed, in 2020, can realize dozens of artificial intelligence functions and achieve excellent results in Multiple international competitions. In 2019, smart voice card swiping system won the start-up capital of ten thousand yuan invested by science and technology enterprises. He has won national inspirational scholarship and first prize scholarship for many times. From 2019 to 2020, he applied for five national patents and authorized five computer soft copyrights. He won the second prize of the National College Students' Internet software design competition, the M prize of MCM, and the second prize of ASC. He has won more than ten provincial and above awards such as the first prize of Hebei College Students' mathematics competition. In 2020, he was approved as the diligent and progressive youth in Hebei Province, and was selected as the national upward good youth. His research area is electronic information engineering.

PING HE was born in Huilongya, Nanchong, China, in November 1990. He received the B.S. degree in automation from the Sichuan University of Science and Engineering, Zigong, Sichuan, China, in June 2012, the M.S. degree in control science and engineering from Northeastern University, Shenyang, Liaoning, China, in July 2014, and the Ph.D. degree in electromechanical engineering from the Universidade de Macau, Taipa, Macau, in June 2017.

From December 2015 to November 2018, he was an Adjunct Associate Professor with the Department of Automation, Sichuan University of Science and Engineering. From August 2017 to August 2019, he was a Postdoctoral Research Fellow with the Emerging Technologies Institute, The University of Hong Kong, and the Smart Construction Laboratory, The Hong Kong Polytechnic University. Since December 2018, he has been a Full Professor with the School of Intelligent Systems Science and Engineering, Jinan University, Zhuhai, Guangdong, China. He has authored two books and more than 50 articles. His research interests include robot, sensor networks, complex networks, multiagent systems, artificial intelligence, control theory, and control engineering.

Dr. He is the Reviewer Member of the Mathematical Reviews of American Mathematical Society. He was a recipient of the Liaoning Province of China Master's Thesis Award for Excellence, in March 2015, and the IEEE Robotics and Automation Society Finalist of Best Paper Award, in July 2018. He also serves as a Section Editor of *Automatika: Journal for Control, Measurement, Electronics, Computing and Communications,* an Academic Editor of *PLOS ONE*, and an Associate Editor of the *Proceedings of the Institution of Mechanical Engineers, Part E: Journal of Process Mechanical Engineering* and IET *The Journal of Engineering*.

XIAOZHEN MA is currently a Sophomore of the Bangor College, Central South University of Forestry and Technology. His research area is electronic information engineering.

In 2019, he won the Successful Participant of Hunan division of China Undergraduate Mathematical Contest in Modeling, and the Successful Participant of Asia and Pacific Mathematical Contest in Modeling.

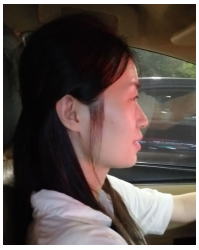

KAI ZHANG was born in Linfen, Shanxi, China, in October 1992. She received the B.S. degree in metallic materials engineering from the Xi'an University of Architecture and Technology, Xi'an, Shaanxi, China, in June 2014, the M.S. degree in material processing engineering from the South China University of Technology, Guangzhou, Guangdong, China, in June 2018.

Since July 2018, she has been a Senior Research and Development Engineer with Yinlong Energy Company, Ltd., Gree Electric Appliances, Inc. of Zhuhai, Guangdong. She has authored some articles. She has also applied three China patents. Her research interests include inorganic materials, material processing, development of lithium-ion battery materials, metallic materials, and electrocatalysis.

HENG LI was born in Hunan, China, in 1963. He received the B.S. and M.S. degrees in civil engineering from Tongji University, in 1984 and 1987, respectively, and the Ph.D. degree in architectural science from The University of Sydney, Australia, in 1993.

From 1993 to 1995, he was a Lecturer with James Cook University. From 1996 to 1997, he was a Senior Lecturer with the Civil Engineering Department, Monash University. Since 1997, he has been gradually promoted from an Associate Professor to a Chair Professor of construction informatics with The Hong Kong Polytechnic University. He has authored two books and more than 500 articles. His research interests include building information modeling, robotics, functional materials, and the Internet of Things.

Dr. Li was a recipient of the National Award from the Chinese Ministry of Education, in 2015, and the Gold Prize of Geneva Innovation, in 2019. He is a Reviews Editor of *Automation in Construction*. He is also an Editorial Board Member of *Advanced Engineering Informatics*.

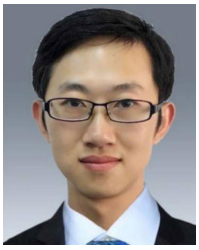

HAOYANG MI received the bachelor's and Ph.D. degrees from the Faculty of Mechanical Engineering, South China University of Technology, Guangzhou, China, in 2010 and 2015, respectively.

From 2016 to 2018, he was a Postdoctoral Researcher with the University of Wisconsin Madison, USA. From 2018 to 2019, he was a Research Fellow with The Hong Kong Polytechnic University. He is currently an Associate Professor with the National Engineering Research Center for Advanced Polymer Processing Technology, Zhengzhou University. He also directs several projects on artificial intelligence and flexible sensors. He has published nearly 100 SCI journal publications so far, with a total citation more than 2000 and an H-index of 27. He has composed a book chapter. He has applied 17 U.S. and China patents. He serves as a regular reviewer for many journals. His current research interests include intelligent materials, artificial intelligence, detection technology, automation device, and flexible sensors.

XINZHONG XIONG received the B.S. degree in communication engineering from the Sichuan University of Science and Engineering, Zigong, China, in 1996, and the M.S. and Ph.D. degrees in communication and information system from the University of Electronic Science and Technology of China (UESTC), in 2006 and 2009, respectively. In 2012, he completed a Research Assignment with the Postdoctoral Station of Electronic Science and Technology, UESTC. He is currently a Professor with the School of Automation and Information Engineering, Sichuan University of Science and Engineering. His research interests include wireless and mobile communications technologies, intelligent signal processing, the Internet-of-Things technologies, and very large-scale integration (VLSI) designs.

ZUXIN LI was born in Zhejiang, China, in 1972. He received the B.S. degree in industrial automation from the Zhejiang University of Technology, China, in 1995, the M.S. degree in communication and information system from Yunnan University, China, in 2002, and the Ph.D. degree in control theory and control engineering from the Zhejiang University of Technology, in 2008.

From May 2009 to March 2013, he was a Postdoctoral Research Fellow with the Institute of Cyber-Systems and Control, Zhejiang University, China. From August to November 2013, he was a Visiting Scholar with Dalhousie University, Canada. He is currently a Full Professor with the School of Engineering, Huzhou University, China. His research interests include networked control systems, robust control, estimation, prognostics, and health management.

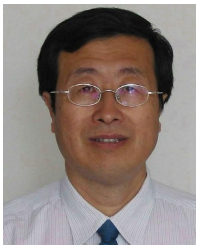

YANGMIN LI (Senior Member, IEEE) received the B.S. and M.S. degrees in mechanical engineering from Jilin University, Changchun, China, in 1985 and 1988, respectively, and the Ph.D. degree in mechanical engineering from Tianjin University, Tianjin, China, in 1994.

He started his academic career, in 1994. He was a Lecturer with the Mechatronics Department, South China University of Technology, Guangzhou, China. From May to November 1996, he was a Fellow with the International Institute for Software Technology, United Nations University (UNU/IIST). He was a Visiting Scholar with the University of Cincinnati, in 1996. He was a Postdoctoral Research Associate with Purdue University, West Lafayette, IN, USA, in 1997. He was an Assistant Professor from 1997 to 2001, an Associate Professor from 2001 to 2007, and a Full Professor from 2007 to 2016, all with the University of Macau. He is currently a Full Professor with the Department of Industrial and Systems Engineering, The Hong Kong Polytechnic University, Hong Kong. He has authored or coauthored more than 400 scientific articles in journals and conferences. His research interests include micro/nanomanipulation, compliant mechanism, precision engineering, robotics, and multibody dynamics and control.

Dr. Li is an Associate Editor of the IEEE TRANSACTIONS ON AUTOMATION SCIENCE AND ENGINEERING, *Mechatrionics*, IEEE ACCESS, and the *International Journal of Control*, *Automation, and Systems*.